Article

Sol–Gel Synthesis of LiTiO$_2$ and LiBO$_2$ and Their CO$_2$ Capture Properties

Liang Li [1,2,]*[ ], Haidi Yu [1] and Yuqi Chen [2,3]

1   School of Mechanical and Electrical Engineering, Nanyang Normal University, Nanyang 473061, China
2   Department of Materials Science and Engineering, Muroran Institute of Technology, Muroran 050-8585, Japan
3   School of Materials Science and Engineering, Shanghai Dian Ji University, Shanghai 201306, China
*   Correspondence: liliangjdgc@nynu.edu.cn; Tel.: +86-037763513077

Abstract: LiTiO$_2$ was prepared from tetraethoxy titanium and lithium ethoxide by a sol–gel process and then treated at 773 K and 973 K under oxygen atmosphere, respectively. Compared with LiTiO$_2$ prepared at 973 K, LiTiO$_2$ prepared at 773 K has better CO$_2$ capture properties. XRD patterns of synthetic LiTiO$_2$ before and after CO$_2$ capture confirm that the intermediate product, Li$_x$Ti$_z$O$_2$, is produced during CO$_2$ capture. CO$_2$ absorption degree of LiTiO$_2$ was determined to be 37% (293 K), 40.8% (333 K), 45.5% (373 K), and 50.1% (393 K) for 11.75 h, respectively. Repetitive CO$_2$ capture experiment indicates that LiTiO$_2$ has excellent cyclic regeneration behavior. The CO$_2$ absorption degree of LiTiO$_2$ increased with increasing CO$_2$ concentration. At a concentration of 0.05%, the absorption degree of LiTiO$_2$ had a stable value of 1% even after an absorption time of 1.4 h. LiBO$_2$ was fabricated by the similar sol–gel method and treated at 713 K. Mass percentage and specific surface area of synthesized LiBO$_2$ increased with the increasing absorption temperature. Evidently, the diffusion of the CO$_2$ molecule through the reaction product, which had a low activation energy of 15 kJ·mol^{-1} and apparent specific surface value of 55.63 m^2/g, determined the efficiency of the absorption reaction. Compared with the other sol–gel synthesized lithium-based oxides, LiTiO$_2$ possessed higher absorption capabilities and lower desorption temperature.

Keywords: LiTiO$_2$; LiBO$_2$; sol–gel synthesis; CO$_2$ capture; rate-determining process

1. Introduction

Solid ceramic absorbents, as one of the most utilized materials for carbon dioxide capture [1,2], have gained more and more attention for their highly cost-effective and energy efficient characteristics for CO$_2$ capturing and sequestration by chemical absorption [3,4]. High-performance absorbents required high selectivity and CO$_2$ absorption capacity, good absorption/desorption kinetics, and stable absorption capacity after repeated cycles. Solid ceramic absorbents include lithium-based ceramic sorbents and sodium-based ceramic sorbents. Sodium-based adsorbents have a high theoretical adsorption capacity and low cost, but have a lower reaction rate and adsorption capacity under actual operating conditions [5–7].

Lithium ceramic absorbents, such as Li$_4$SiO$_4$ [4,8–11], Li$_2$ZrO$_3$ [12–14], and Li$_2$MnO$_3$ [15], had displayed high CO$_2$ absorption capacity [16] and ultrafast carbon dioxide sorption kinetics [17]. The development of novel materials for CO$_2$ capture is one of the important themes in adsorption science [18]. It is meaningful to study CO$_2$ capture properties of LiTiO$_2$ and LiBO$_2$ for the prominent CO$_2$ absorbent materials because they can react with CO$_2$ reversibly. Compared with other CO$_2$ absorbers, another advantage for lithium ceramic absorbents is that different absorption thermodynamic equilibrium temperatures expand the CO$_2$ capture temperature range so these corresponding oxides can be applied for different temperatures [16].

CO$_2$ absorption properties of those compounds were not only influenced by the constituents but also the synthesis methods [19]. Li$_4$SiO$_4$ has been prepared by one-step

synthesis [20–22] or the sample rolling ball method [11,23]. $LiTiO_2$ has been synthesized by mechanochemical reactions between Li_2O, Ti, and TiO_2 by ball milling [24], the electrochemical insertion of Li^+ into TiO_2 in a fused LiCl salt medium [25], the hydrothermal method [26], microwave heating of the mixture of Li_2CO_3 and TiO_2 [27] method, and so on. When compared to conventional techniques, sol–gel polymerization synthesis offers superior control over the production of fine powders of better purity at low temperatures and requires just basic tools and procedures [28].

In our former research, Li_2ZrO_3 and Li_2SiO_3 have been fabricated by sol–gel process [29,30]. CO_2 absorption degree of synthesized Li_2ZrO_3 was higher than that of solid-state synthesized Li_2ZrO_3 [29]. Therefore, sol–gel synthesized $LiTiO_2$ and $LiBO_2$ are speculated to exhibit similar CO_2 absorption characteristics of Li_2ZrO_3 [31]. However, synthesis of $LiTiO_2$ and $LiBO_2$ by a similar sol–gel process has little been reported.

In this study, $LiTiO_2$ and $LiBO_2$ powders were synthesized by the sol–gel process. The reversible reactions between $LiTiO_2$ and $LiBO_2$ and CO_2 are listed below. CO_2 absorption properties and cyclic behavior of $LiTiO_2$ were evaluated by dynamic and isothermal thermogravimetry analysis. CO_2 capture properties and the specific surface area of $LiBO_2$ were evaluated with chromatography and the BET method, respectively. Kinetic of CO_2 absorption/desorption processes of $LiTiO_2$ was analyzed with different kinetic equations. CO_2 capture properties of sol–gel synthesized lithium ceramic absorbents were compared and summarized.

$$2\ LiTiO_2 + CO_2 = Li_2CO_3 + Ti_2O_3 \tag{1}$$

$$2\ LiBO_2 + CO_2 = Li_2CO_3 + B_2O_3 \tag{2}$$
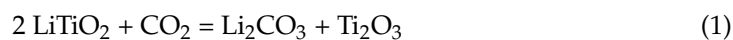
2. Materials and Methods

2.1. Sol–Gel Synthesis Processes of LiTiO₂ and LiBO₂

The sol–gel synthesis processes of $LiTiO_2$ and $LiBO_2$ are described as follows. The preparation of sol was conducted under dry N_2 atmosphere because sol is extremely sensitive to moisture. Table 1 lists the starting material information and molar ratio for the synthesis of $LiTiO_2$ and $LiBO_2$. Firstly, $Ti(OC_2H_5)_4$ or $B(i\text{-}OC_3H_7)_3$ was dissolved by stirring in the mixture of $(C_2H_4OH)_2O$ and a quarter of C_2H_5OH. Then, drop by drop, distilled water containing another quarter of C_2H_5OH was stirred into the aforementioned solution until it was clear. In another container, $LiOC_2H_5$ was incorporated in 50 percent of the C_2H_5OH solution by swirling. The molar ratio of Li:B was designed to be 3:2 in order to compensate for the loss of Li atoms during the preparation of the $LiBO_2$ solvate precursors. Finally, clear lithium precursor solution was slowly added to the titanium precursor solution. These solutions were mixed by stirring and then aged for 24 h at room temperature.

Table 1. Raw material information and molar ratio for synthesis of $LiTiO_2$ and $LiBO_2$.

Reagent	Chemical Formula	$LiTiO_2$	$LiBO_2$
Tetra-ethoxytitanium	$Ti(OC_2H_5)_4$	1	–
Tri-isopropoxyboron	$B(i\text{-}OC_3H_7)_3$	–	2
Lithium ethoxide	$LiOC_2H_5$	1	3
Ethanol	C_2H_5OH	200	50
Diethylene glycol	$(C_2H_4OH)_2O$	10	3
Distilled water	H_2O	5	6

The gel was produced by vacuum curing the sol in a Petri plate at room temperature for 48 h. To hasten the breakdown of organic residues, the wet gel was heated to 773 K (or 973 K) for the preparation of $LiTiO_2$ and 713 K for the preparation of $LiBO_2$ with duration of 0.5 h under a flow of oxygen gas, respectively. The resultant powder was ground gently by an agate mortar to break the agglomerates. Lastly, the ground powder was heated to

623 K for an absorption time of 0.3 h under Ar atmosphere to remove the absorbent CO_2 during the synthesis process.

2.2. Characterization

The synthesized powders were characterized through the utilization of X-ray diffraction (XRD: Rint-Ultima+, Rigaku Corp., Tokyo, Japan) with monochromatic CuKα radiation. On a surface area analyzer (Autosorb-1, Quantachrome, Boynton Beach, FL, USA), the Brunauer–Emmett–Teller (BET) technique was used to measure the specific surface areas (SSA) of synthesized powders.

CO_2 capture properties of $LiTiO_2$ and $LiBO_2$ were evaluated simultaneously by thermogravimetry and differential thermal analysis (TG-DTA2000S, MAC Science Co., Ltd., Kanagawa, Japan). To determine the CO_2 capture temperatures, the produced $LiTiO_2$ powder was heated from ambient temperature to 623 K continuously at 10 °C·min^{-1} under 300 mL/min of dry CO_2 flowing. To understand the repetitive CO_2 absorption properties, the samples were heated to 388 K at a rate of 5 °C/min for 0.9 h under CO_2 atmosphere after heating at 623 K under Ar atmosphere and cooling to ambient. These steps were repeated five times.

Absorption degree is calculated by multiplying the proportion weight of $LiTiO_2$ or $LiBO_2$ added following absorbing by the percentage amount added to equate to 100% reaction completion of the reaction, as shown in Equations (1) and (2). The degree of absorption was calculated with the mathematical formula Equation (3):

$$R = (M_2 - M_1)/M_1\alpha \tag{3}$$

where R represents absorption degree (%); M_1 and M_2 are sample mass (mg) before and after CO_2 absorption, respectively. The factor α is a value of $LiTiO_2$/$LiBO_2$ mass required to absorb one mole of CO_2 divided by the molecular mass of CO_2. The estimated value of α is 0.253 for $LiTiO_2$ and 0.44 for $LiBO_2$.

To investigate the influence of CO_2 concentration on the absorption degree of $LiTiO_2$, the synthesized $LiTiO_2$ powder was heated to 388 K at a rate of 5 °C·min^{-1} in a gas mixture of CO_2 and N_2 gas with a flowing rate of 300 mL/min. The mixture ratio of CO_2 was 0.05% (500 ppm, which is close to CO_2 concentration of the ambient atmosphere), 10%, 40%, and 100%, respectively. $LiBO_2$ was evaluated with the mixture gas of N_2 and CO_2 (volume ratio = 6:4) by the gas chromatography method to check the variation of CO_2 concentration with time. The sample was placed in the sample holder in the furnace and the mixture gas flowed into the furnace from the right (primary gas) and left side (secondary gas). The primary gas pressure was 0.1 MPa and gas flowing rate was 500 mL/min. The secondary gas flowing rate was 30 mL/min.

3. Results

3.1. Synthesis of LiTiO₂ and LiBO₂ Powders

Figure 1 depicts TG-DTA trends for the chemically synthesized products heated to 623 K in a CO_2 environment as the second heat treatment. The samples were prepared by heating the gel at 773 K (marked as $LiTiO_2$-A) and 973 K (marked as $LiTiO_2$-B), respectively. $LiTiO_2$-A and $LiTiO_2$-B showed similar TG behavior as the temperature increased. TG of $LiTiO_2$-A increased gradually with a temperature up to approximately 360 K and subsequently decreased immediately at 360–573 K. The remarkable rise and decline of mass of $LiTiO_2$-A corresponded to CO_2 absorption and desorption. Above 573 K, the value of mass loss transfer changed from positive to negative. The difference in the amount of CO_2 before absorption and after desorption can be attributed to the characteristics of the sol–gel synthesized powders. A carbonated phase is said to have formed when heat treatment breaks down any remaining organic materials in wet gels.
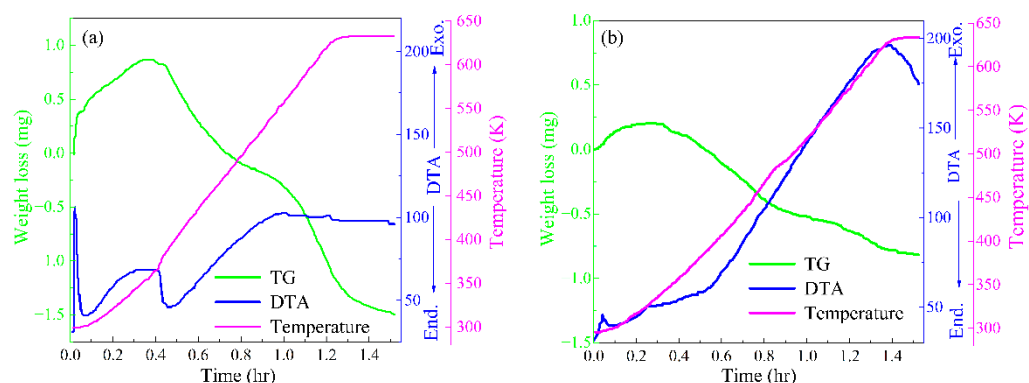
Figure 1. TG-DTA curves of sample prepared by heating the gel at 773 K (**a**) and 973 K (**b**) under CO_2 atmosphere.

DTA curve of $LiTiO_2$-A showed a strong endothermic peak at the beginning of the reaction, indicating CO_2 absorption, while $LiTiO_2$-B exhibited a relatively low endothermic DTA peak. At approximately 360 K, the mass loss of $LiTiO_2$-A reached its maximum of 0.9 mg, which is 4.5 times higher than that of $LiTiO_2$-B (0.2 mg at 330 K), revealing that $LiTiO_2$-A has better CO_2 capture property than that of $LiTiO_2$-B. For this reason, the gel was heated at 773 K in the subsequent experiment.

Figure 2 displays the TG-DTA profiles for the synthetic products heated to 650 K in an environment of Ar. The mass of $LiTiO_2$-A decreased at above 320 K, which was lower than that treated under CO_2 atmosphere (360 K), as shown in Figure 1a. Table 2 lists the weight losses of sample prepared by heating the gel at 773–973 K. This mass loss may potentially be related to CO_2 desorption, which results from the initial remaining organic component's dissociation. The decomposition temperature of carbonates decreases with the fall of CO_2 partial pressure under the Ar atmosphere. Both the TG and DTA curve also saturate to a constant at 630 K, and there is no further drop in mass beyond 623 K under the Ar atmosphere. Therefore, all the adsorbent CO_2 can be assumed to be released at 623 K. Hence, CO_2 capture properties were studied after heating the samples to 623 K under an Ar atmosphere.
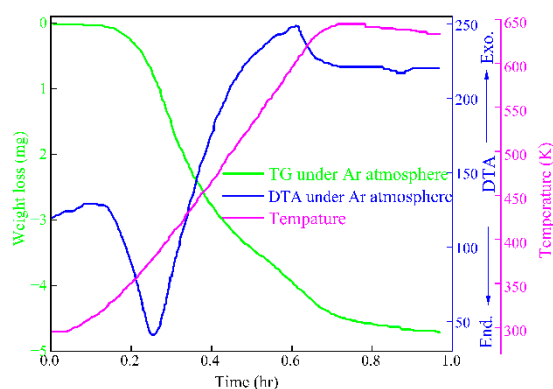
Figure 2. TG-DTA curves of sample prepared by heating the gel at 773 K under Ar atmosphere.

Table 2. Weight losses of sample prepared by heating the gel at 773–973 K.

Temperature (K)	Atmosphere	Weight Losses (mg)
773	CO_2	1.5
973	CO_2	0.8
773	Ar	4.7

XRD patterns of synthetic $LiTiO_2$ before and after CO_2 absorption are shown in Figure 3. This sample reacted with CO_2 at 373 K for 11.75 h for the absorption degree of 43%, which will be discussed later in detail. Before CO_2 absorption, diffraction peaks corresponding to single $LiTiO_2$ have been confirmed in Figure 3a. During CO_2 adsorption, the intermediate product $Li_xTi_zO_2$ is generated (Figure 3b) and after five cycles of adsorption $LiTiO_2$ is re-formed (Figure 3c).
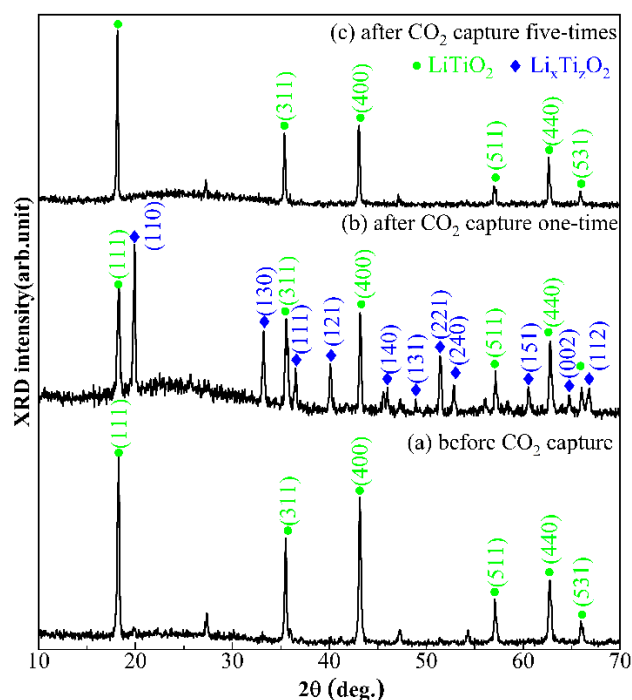
Figure 3. XRD patterns of synthetic $LiTiO_2$ before and after CO_2 absorption.

The SSA of $LiTiO_2$ before and after CO_2 absorption was found to be 55.63 and 61.56 $m^2 \cdot g^{-1}$, respectively. If we assume that the mass of $LiTiO_2$ is 188 g, the system theory volume can be calculated according to the density of $LiTiO_2$ (3.15 $g \cdot cm^{-3}$). Similarly, the system volume after CO_2 absorption is calculated with the densities of $LiCO_3$ and Ti_2O_3 (2.11 and 4.49 $g \cdot cm^{-3}$, respectively). The system theory volume increased by 11% following with CO_2 absorption progress, indicating that SSA of $LiTiO_2$ should be enlarged during the CO_2 absorption process.

3.2. CO_2 Absorption Properties of $LiTiO_2$ and $LiBO_2$

Figure 4 shows the absorption curves of $LiTiO_2$ for an absorption time of 11.75 h obtained from TG. The temperature increased with a rate of 5 $°C \cdot min^{-1}$ and then maintained at 293 K, 333 K, 373 K, and 393 K, respectively. As shown in Table 3, the absorption degree attained 37%, 40.8%, 45.5%, and 50.1% at the maintained temperature of 293 K, 333 K, 373 K, and 393 K, respectively. CO_2 absorption degrees of sol–gel synthesized Li_2ZrO_3 were also considered for comparison [29]. The CO_2 absorption degree of Li_2ZrO_3 only attained 17%, 20%, and 22% at the same conditions [29].
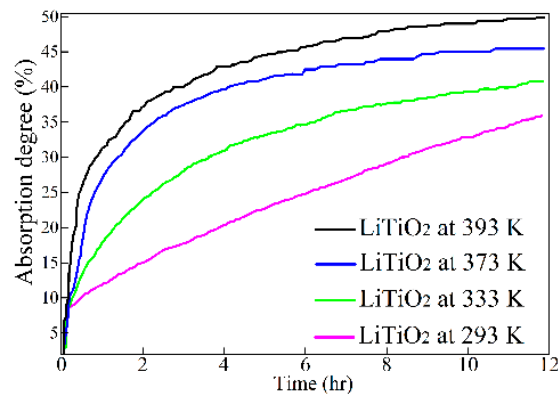
Figure 4. Comparison absorption degree of CO_2 between $LiTiO_2$.

Table 3. Absorption degree of $LiTiO_2$ at 293K–393 K for the absorption time of 2–11.75 h.

Temperature (K)	Abs. 2 (h)	Abs. 4 (h)	Abs. 8 (h)	Abs. 11.75 (h)
293	14.9	20.3	29.1	37.0
333	23.9	31.0	37.7	40.8
373	33.5	39.8	44.0	45.5
393	37.2	42.9	48.0	50.1

Repetitive CO_2 absorption degree of $LiTiO_2$ was obtained from TG analysis as shown in Figure 5. The repetitive CO_2 absorption degree decreased slightly every time with a mean drop of 0.5%. As shown in Table 4, the absorption degree of $LiTiO_2$ decreases with the increasing number of cycles. This result is similar with that of sol–gel synthesized Li_2ZrO_3 [29].
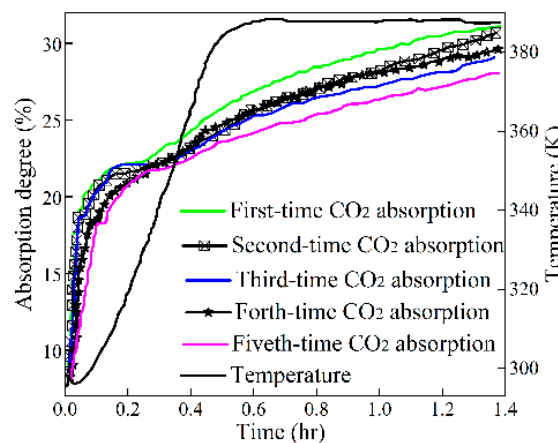
Figure 5. Repetitive cycles absorption on absorption degree of $LiTiO_2$.

Table 4. Absorption degree of $LiTiO_2$ for the repetitive cycles.

CO_2 Absorption	Abs. 0.2 (h)	Abs. 0.6 (h)	Abs. 1.0 (h)	Abs. 0.14 (h)
First time	22.2	26.9	29.6	31.3
Second time	21.6	25.7	28.2	30.7
Third time	22.1	25.2	27.3	29.1
Fourth time	21.0	25.6	28.0	29.6
Fifth time	20.8	24.1	26.4	28.1

Figure 6 shows the influence of variation of CO_2 concentration on the absorption degree of $LiTiO_2$ at different temperatures. As shown in Table 5, the absorption degree

enlarges with the augmentation of CO_2 concentration. The absorption degree of $LiTiO_2$ is approximately 30% under pure CO_2 atmosphere. Moreover, the absorption degree of $LiTiO_2$ decreases from 25% to 23% as CO_2 concentration reduces from 40% to 10%. Finally, the absorption degree is a minuscule 1% even after an absorption time of 1.4 h at a CO_2 concentration of 0.05%.
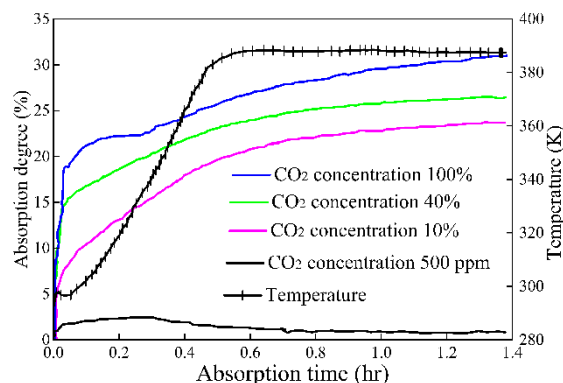
Figure 6. Dependence of CO_2 concentrations on the absorption degree of $LiTiO_2$.

Table 5. Dependence of the concentrations of CO_2 in the atmosphere on the degree of absorption.

CO_2 Absorption	Abs. 0.2 (h)	Abs. 0.6 (h)	Abs. 1.0 (h)	Abs. 0.14 (h)
500 ppm	2.4	1.3	0.9	0.9
10%	13.1	20.7	22.8	23.7
40%	18.6	24.0	25.8	26.4
100%	22.3	26.9	29.6	31.3

The mass percentage of synthetic $LiBO_2$ at 333–423 K is shown in Figure 7. As shown in Table 6, the mass percentage of synthetic $LiBO_2$ enlarged with the augment of CO_2 absorption temperature. $LiBO_2$ reacted with CO_2 with the extension of the absorption time. Higher explored temperatures improved the reaction activation energy and then increased the mass percentage of $LiBO_2$. The mass percentage of synthetic $LiBO_2$ at 393 and 423 K presents a second mass increment in the last part of these curves. Usually, similar behaviors have been associated with physical adsorption. Therefore, absorption of $LiBO_2$ is the mixture of both the physical adsorption and chemical absorption of CO_2. Table 7 lists the specific surface area and mass percentage of synthetic $LiBO_2$. Following the increasing absorption temperature, SSA of synthetic $LiBO_2$ obviously increased. SSA of synthetic $LiBO_2$ is larger than that of Li_2ZrO_3 (SSA value of 6.9 m^2/g). Similar to $LiBO_2$, Li_3BO_3 exhibits exceptionally quick kinetics and a high ability to collect CO_2 [32].
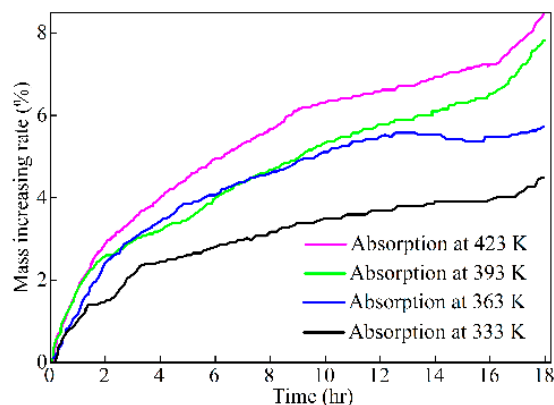
Figure 7. Weight percentage of synthetic $LiBO_2$ at 333–423 K.

Table 6. Mass increasing rate of $LiBO_2$ at 333–423 K for the absorption time of 6–18 h.

Temperature (K)	Abs. 6 (h)	Abs. 12 (h)	Abs. 18 (h)
333	2.8	3.7	4.5
363	4.1	5.5	5.8
393	4.0	5.8	7.9
423	5.0	6.6	8.5

Table 7. Specific surface area and weight percentage of synthetic $LiBO_2$.

Temperature (K)	Weight Percentage (%)	SSA (m^2/g)
293	0	12.2
333	4.5	16.8
363	5.7	30.5

Figure 8 shows the evaluation of CO_2 absorption properties of $LiBO_2$ with the gas chromatography method. As the absorption time extended, CO_2 concentrations lessened firstly and then reached a saturation value at 363 K and 393 K. As shown in Table 8, higher absorption temperatures can shorten the absorption time for saturation, which is the same as the result of mass percentage (Figure 7). However, the variation of CO_2 concentration for the absorption at 363 K is larger than that for the absorption at 393 K because the equilibrium temperature of $LiBO_2$ is 333 K.
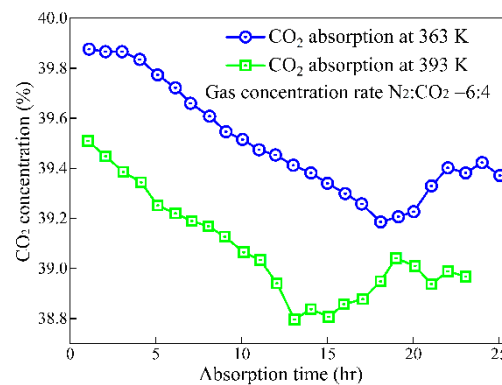
Figure 8. Evaluation of CO_2 absorption properties of $LiBO_2$ with gas chromatography method.

Table 8. Evaluation of CO_2 absorption properties of $LiBO_2$ with gas chromatography method.

Temperature (K)	Abs. 5 (h)	Abs. 10 (h)	Abs. 15 (h)	Abs. 20 (h)
363	39.8	39.5	39.3	39.2
393	39.3	39.0	38.8	39.0

3.3. Kinetic Calculation Analysis

The kinetic consecutive reaction model for CO_2 capture on lithium ceramic absorbents was connected with the CO_2 flow rate [33]. The conversion kinetics for the interaction combining $LiTiO_2$ and CO_2 are shown in Figure 9. This reaction mechanism for $LiTiO_2$ was similar to the reported model of high-temperature CO_2 capture on Li_2ZrO_3 [34,35]. The following rate equations were employed for analyzing the experimental data, as shown in Figure 4:

(1) equations generated from mobility modeling procedures where gas diffusion through the Li_2CO_3 and Ti_2O_3 layer is the rate-limiting phase, especially, the Yander formula [36], $Y_1 = (1 - (1 - R)^{1/3})^2 = kt$; and Gistling model [37], $Y_2 = 1 - 2\alpha/3 - (1 - \alpha)^{2/3} = kt$;

(2) equation for reactions in cylinder-shaped particles that are constrained by interfacial processes, $Y_1 = 1 - (1 - \alpha)^{1/2} = kt$; and $Y_2 = 1 - (1 - \alpha)^{1/3}$.
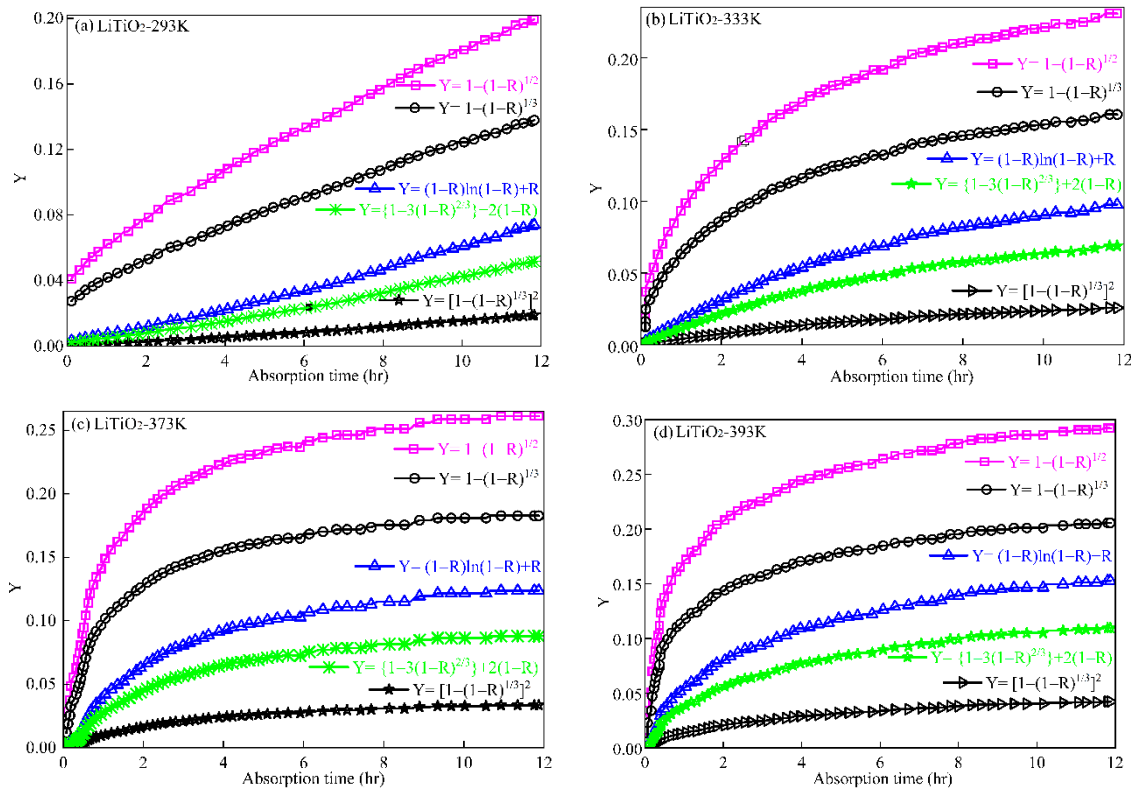
Figure 9. Plot of reaction kinetics and absorption time at 293 K (**a**), 333 K (**b**), 373 K (**c**), and 393 K (**d**) for data from Figure 4.

In Figure 9, data analysis shows that the highest correlation coefficient is achieved between 293 K and 393 K when the Yander equation [38] and Gistling equation [39] are fit. The formula of interactions restricted by contact processes just fits for the absorption at low temperature (293 K) and fails at high temperature due to the change of shape of the $LiTiO_2$ particle and the thickness of the product layer. These equations apply only for a sphere when the radius is very large as compared with the thickness of the product layer. An approximately linear dependence is found to a relatively high absorption degree. Therefore, the rate-determining step might be the gas diffusion in the Li_2CO_3 and Ti_2O_3 layer.

The Gistling equation is provided below [39]:

$$1 - 3(1 - R)^{2/3} + 2(1 - R) = (2MDC/\alpha\rho r_0{}^2) = k't \qquad (4)$$

where R denotes the percentage of absorption, (%); M is the reactant's molecular mass, $(g \cdot mol^{-1})$; D is the intra-particle efficient diffusivity, $(cm^2 \cdot s^{-1})$; C stands for the reagent concentration; α means the stoichiometric ratio; ρ indicates the reactant density; r_0 is the reactant's initial particle diameter, (cm); t is the reaction time, (s); and k' is the rate parameter.

Accorded to Equation (4), the values of rate constant k' are calculated. Rate constant k' showed linear temperature dependence. The effective kinetic energy (ΔE) is determined from the values of the slope and is calculated as 15 $kJ \cdot mol^{-1}$. This value is slightly smaller than that of sol–gel synthesized Li_2ZrO_3 (24 $kJ \cdot mol^{-1}$ [40]). As a further comparison, the apparent activation energy of zeolite pores with the approximate diameter of 0.4 nm is approximately 20 $kJ \cdot mol^{-1}$ during CO_2 diffusion through [41]. The rate-determining step of CO_2 capture in the instance of $LiTiO_2$ is likewise assumed to be its dispersion in the chemical process of diffusion.

3.4. Evaluation of CO$_2$ Capture Properties of Sol–Gel Prepared Lithium Ceramic Absorbents

Figure 10 shows a comparison of mass percentage of sol–gel synthesized lithium ceramic absorbents at 333K. Compared with other lithium ceramic absorbents, LiTiO$_2$ has the maximal mass percentage as shown in Table 9. It might be attributed to the larger specific surface area SSA (Table 3) and lower activation energy of sol–gel synthesized LiTiO$_2$. On comparison of the ambient temperature CO$_2$ absorption properties of LiTiO$_2$ and Li$_2$ZrO$_3$ powders [29] synthesized by the same sol–gel process, the absorption degree of LiTiO$_2$ was two times higher than that of Li$_2$ZrO$_3$. This difference should be attributed to the major difference in specific surface areas of 55.63 m^2·g^{-1} of LiTiO$_2$ as compared with 12.25 m^2·g^{-1} of Li$_2$ZrO$_3$, determined before CO$_2$ absorption.
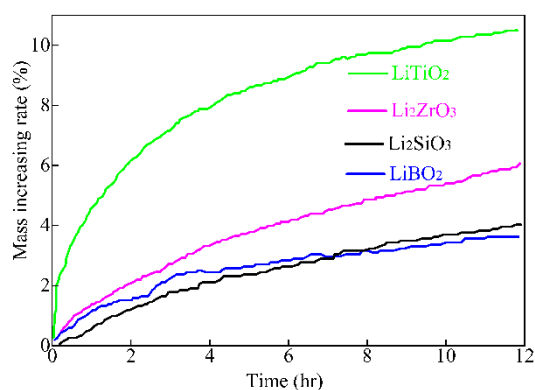
Figure 10. Comparison of weight percentage of sol–gel synthesized lithium-based oxides at 333 K.

Table 9. Mass increasing rate of lithium-based oxides for the absorption time of 2–11.75 h.

Temperature (K)	Abs. 2 (h)	Abs. 4 (h)	Abs. 8 (h)	Abs. 11.75 (h)
LiTiO$_2$	6.1	7.9	9.7	10.5
Li$_2$ZrO$_3$	2.1	3.3	4.8	6.0
Li$_2$SiO$_3$	1.2	2.1	3.2	4.1
LiBO$_2$	1.5	2.5	3.1	3.6

Table 10 summarizes the CO$_2$ capture properties of lithium ceramic absorbents synthesized by the sol–gel method. These lithium ceramic absorbents, which have different CO$_2$ emission temperatures, can be employed at an altered temperature range. LiTiO$_2$ has the highest CO$_2$ absorptivity and largest mass percentage among these lithium ceramic absorbents due to its smallest activation energy. The equilibrium temperature of LiTiO$_2$ (393 K) is considerably lower than that of Li$_2$ZrO$_3$ (992 K), indicating that LiTiO$_2$ is easier to renew compared with Li$_2$ZrO$_3$; that is, LiTiO$_2$ is a more efficient CO$_2$ absorption material than Li$_2$ZrO$_3$. The sol–gel synthesized LiTiO$_2$ powders can be employed as a solid CO$_2$ sorbent at near-ambient temperatures.

Table 10. CO$_2$ capture properties of lithium-based oxides synthesized by sol–gel method.

Property	Li$_2$ZrO$_3$ [29]	Li$_2$SiO$_3$ [30]	Li$_4$SiO$_4$	LiTiO$_2$	LiBO$_2$
CO$_2$ emission temp.(K)	923	593	643	393	333
CO$_2$ absorptivity (%) room T	23	8	–	38	–
Weight percentage (%)	5	4	3	10	4
SSA (m^2/g)	6.9	40.6	3.1	55.6	12.2
SSA (m^2/g) (after absorption)	–	–	–	61.56	–
Activation energy (kJ/mol)	24	28	–	–	

4. Conclusions

The preparation process of $LiTiO_2$ and $LiBO_2$ by a sol–gel process was investigated. $LiTiO_2$ and $LiBO_2$ with a larger SSA were fabricated by this method. The variety of TG-DTA revealed that $LiTiO_2$ prepared at 773 K has better CO_2 capture property, especially at approximately room temperature. The reaction between $LiTiO_2$ and CO_2 is reversible with an equilibrium temperature of 500 K. $LiTiO_2$ showed excellent repeated cyclic absorption behavior for CO_2 absorption and desorption. The absorption degree of $LiTiO_2$ reached 50.1% at 393 K for 11.75 h. The repetitive CO_2 absorption degree experiment indicates that CO_2 absorption degree decreased slightly every time with a mean decrease of 0.5%. The absorption degree of $LiTiO_2$ lessened with the diminution of CO_2 concentration. At a CO_2 concentration of 0.05%, the $LiTiO_2$ showed a low CO_2 absorption degree but kept a stable absorption degree of 1% as time went on. Higher absorption temperature increased the mass percentage and specific surface area of synthetic $LiBO_2$. The absorption behavior could be well explained by an intra-particle diffusion mechanism. The rate-determining step is CO_2 diffusion through the Li_2CO_3 and Ti_2O_3 layer with activation energy of 15 kJ·mol^{-1}, which is slightly smaller than that of Li_2ZrO_3 prepared by the same sol–gel process.

Author Contributions: Formal analysis, L.L.; investigation, L.L. and Y.C.; data curation, L.L., H.Y. and Y.C.; writing—original draft preparation, L.L. and Y.C.; writing—review and editing, L.L. and Y.C.; supervision, L.L.; funding acquisition, L.L.; All authors have read and agreed to the published version of the manuscript.

Institutional Review Board Statement: Not applicable.

Informed Consent Statement: Not applicable.

Data Availability Statement: The data presented in this study are available on request from the corresponding author.

Conflicts of Interest: The authors declare no conflict of interest. The authors declare that they have no known competing financial interest or personal relationships that could have appeared to influence the work reported in this paper.

References

1. Yaumi, A.; Bakar, M.A.; Hameed, B. Recent advances in functionalized composite solid materials for carbon dioxide capture. *Energy* **2017**, *124*, 461–480. [CrossRef]
2. Supriya, N.; Rajeev, R. Synthesis and characterization of lithium silicates from organosilicone precursors for carbon dioxide adsorption. *J. Therm. Anal. Calorim.* **2020**, *147*, 135–143. [CrossRef]
3. Deng, B.; Tang, J.; Mao, X.; Song, Y.; Zhu, H.; Xiao, W.; Wang, D. Kinetic and thermodynamic characterization of enhanced carbon dioxide absorption process with lithium oxide-containing ternary molten carbonate. *Environ. Sci. Technol.* **2016**, *50*, 10588–10595. [CrossRef]
4. Yin, Z.; Wang, K.; Zhao, P.; Tang, X. Enhanced CO_2 chemisorption properties of Li_4SO_4, using a water hydration–calcination technique. *Ind. Eng. Chem. Res.* **2016**, *55*, 1142–1146. [CrossRef]
5. Wu, Y.; Liu, W. Element doped sodium-based sorbents with high attrition resistance and CO_2 capture capacity during CO_2 sorption/desorption processes. *Fuel* **2021**, *285*, 119165. [CrossRef]
6. Kar, S.; Goeppert, A.; Galvan, V.; Chowdhury, R.; Olah, J.; Prakash, G.S. A carbon-neutral CO_2 capture, conversion, and utilization cycle with low-temperature regeneration of sodium hydroxide. *J. Am. Chem. Soc.* **2018**, *140*, 16873–16876. [CrossRef] [PubMed]
7. Ji, G.; Yang, H.; Memon, M.Z.; Gao, Y.; Qu, B.; Fu, W.; Olguin, G.; Zhao, M.; Li, A. Recent advances on kinetics of carbon dioxide capture using solid sorbents at elevated temperatures. *Appl. Energy* **2020**, *267*, 114874. [CrossRef]
8. Wang, K.; Li, W.; Yin, Z.; Zhou, Z.; Zhao, P. High-capacity Li_4SO_4-based CO_2 Sorbents via a facile hydration-NaCl doping technique. *Energy Fuels* **2017**, *31*, 6257–6265. [CrossRef]

9. Takasu, H.; Ryu, J.; Kato, Y. Application of lithium orthosilicate for high-temperature thermochemical energy storage. *Appl. Energy* **2017**, *193*, 74–83. [CrossRef]

10. Subha, P.; Nair, B.N.; Visakh, V.; Achu, R.; Shikhila, S.; Mohamed, A.P.; Yamaguchi, T.; Hareesh, U. Wet chemically derived Li_4SO_4 nanowires as efficient CO_2 sorbents at intermediate temperatures. *Chem. Eng. J.* **2021**, *406*, 126731. [CrossRef]

11. Sanna, A.; Thompson, S.; Zajac, J.; Whitty, K. Evaluation of palm-oil fly ash derived lithium silicate for CO_2 sorption under simulated gasification conditions. *J. CO2 Util.* **2022**, *56*, 101826. [CrossRef]

12. Alcántar-Vázquez, B.; Duan, Y.; Pfeiffer, H. CO oxidation and subsequent CO_2 chemisorption on alkaline zirconates: Li_2ZrO_3 and Na_2ZrO_3. *Ind. Eng. Chem. Res.* **2016**, *55*, 9880–9886. [CrossRef]

13. Jo, H.G.; Yoon, H.J.; Lee, C.H.; Lee, K.B. Citrate sol–gel method for the preparation of sodium zirconate for high-temperature CO_2 sorption. *Ind. Eng. Chem. Res.* **2016**, *55*, 3833–3839. [CrossRef]

14. Orsetti, N.G.; Gamba, M.; Gómez, S.; Gaviria, J.P.Y.; Suarez, G. The transcendental role of lithium zirconates in the development of modern energy technologies. *Ceram. Int.* **2022**, *48*, 8930–8959. [CrossRef]

15. Hernández-Fontes, C.; Pfeiffer, H. Unraveling the CO and CO_2 reactivity on Li_2MnO_3: Sorption and catalytic analyses. *Chem. Eng. J.* **2022**, *428*, 131998. [CrossRef]

16. Kumar, S.; Saxena, S.K. A comparative study of CO_2 sorption properties for different oxides. *Mater. Renew. Sustain. Energy* **2014**, *3*, 30. [CrossRef]

17. Nambo, A.; He, J.; Nguyen, T.Q.; Atla, V.; Druffel, T.L.; Sunkara, M.K. Ultrafast carbon dioxide sorption kinetics using lithium silicate nanowires. *Nano Lett.* **2017**, *17*, 3327–3333. [CrossRef]

18. D'Alessandro, D.M.; Smit, B.; Long, J.R. Carbon dioxide capture: Prospects for new materials. *Angew. Chem. Int. Ed.* **2010**, *49*, 6058–6082. [CrossRef]

19. Hu, Y.; Fu, R.; Liu, W.; Yao, D.; Yan, S. Lithium-based ceramics in nonsilicates for CO_2 capture: Current status and new trends. *J. Mater. Chem. A* **2022**, *10*, 1706–1725. [CrossRef]

20. Stefanelli, E.; Vitolo, S.; Puccini, M. Single-step fabrication of templated Li_4SiO_4-based pellets for CO_2 capture at high temperature. *J. Environ. Chem. Eng.* **2022**, *10*, 108389. [CrossRef]

21. Hu, Y.; Fu, R.; Yu, G.; Cao, J.; Huang, J. Scalable synthesis of Li_4SiO_4 sorbent from novel low-cost orthoclase mineral for CO_2 capture. *Fuel* **2022**, *324*, 124492. [CrossRef]

22. Fu, R.; Yu, G.; Cheng, J.; Hu, Y.; Yan, S. One-step synthesis of porous Li_4SiO_4 pellets by polyvinyl alcohol (PVA) method for CO_2 capture. *Fuel* **2023**, *331*, 125873. [CrossRef]

23. Tan, G.; Hu, X.; Wang, C.; Cai, L.; Song, S.; Nong, Y.; Wang, Q.; Ren, Y.; Yang, X.; Zhang, Y. High efficiency CO_2 sorption property of Li_4SiO_4 sorbent pebbles via a simple rolling ball method. *Sep. Purif. Technol.* **2022**, *298*, 121662. [CrossRef]

24. Obrovac, M.N.; Mao, O.; Dahn, J.R. Structure and electrochemistry of $LiMO_2$ (M= Ti, Mn, Fe, Co, Ni) prepared by mechanochemical synthesis. *Solid State Ion.* **1998**, *112*, 9–19. [CrossRef]

25. Jiang, K.; Hu, X.; Sun, H.; Wang, D.; Jin, X.; Ren, Y.; Chen, G.Z. Electrochemical synthesis of $LiTiO_2$ and $LiTi_2O_4$ in molten LiCl. *Chem. Mater.* **2004**, *16*, 4324–4329. [CrossRef]

26. Zhang, D.R.; Liu, H.L.; Jin, R.H.; Zhang, N.Z.; Liu, Y.X.; Kang, Y.S. Synthesis and characterization of nanocrystalline $LiTiO_2$ using a one-step hydrothermal method. *J. Ind. Eng. Chem.* **2007**, *13*, 92–96.

27. Yang, L.H.; Dong, C.; Guo, J. Hybrid microwave synthesis and characterization of the compounds in the Li–Ti–O system. *J. Power Sources* **2008**, *175*, 575–580. [CrossRef]

28. Yoldas, B.E. Technological significance of sol-gel process and process-induced variations in sol-gel materials and coatings. *J. Sol-Gel Sci. Technol.* **1993**, *1*, 65–77. [CrossRef]

29. Wang, F.; Yoshimura, Y.; Hirai, S.; Kuzuya, T. CO_2 absorption/release properties of lithium zirconate powder prepared by the sol-gel process. *Resour. Processes* **2011**, *58*, 108–113. [CrossRef]

30. Wang, F.; Wakou, S.; Hirai, S.; Kuzuya, T.; Li, T. CO_2 absorption/release properties of lithium silicate (Li_2SiO_3) powders prepared by the sol-gel process. *Appl. Mech. Mater.* **2014**, *675*, 7–14.

31. Deptuła, A.; Olczak, T.; Łada, W.; Sartowska, B.; Chmielewski, A.G.; Alvani, C.; Carconi, P.L.; Di Bartolomeo, A.; Pierdominici, F.; Casadio, S. Inorganic sol-gel preparation of medium sized microparticles of Li_2TiO_3 from $TiCl_4$ as tritium breeding material for fusion reactors. *J. Sol-Gel Sci. Technol.* **2003**, *26*, 207–212. [CrossRef]

32. Villa-Pérez, C.; Larochette, P.A.; Soria, D.B.; Gennari, F.C. Thermodynamic and kinetic properties of Li_3BO_3 modified by the alkali fluorides addition in the CO_2 capture process. *Chem. Eng. J.* **2022**, *450*, 138118. [CrossRef]

33. Mendoza-Nieto, J.A.; Martínez-Hernández, H.; Pfeiffer, H.; Gómez-García, J.F. A new kinetic model for CO_2 capture on sodium zirconate (Na_2ZrO_3): An analysis under different flow rates. *J. CO2 Util.* **2022**, *56*, 101862. [CrossRef]

34. Ida, J.-i.; Lin, Y. Mechanism of high-temperature CO_2 sorption on lithium zirconate. *Environ. Sci. Technol.* **2003**, *37*, 1999–2004. [CrossRef]

35. Guo, X.; Ding, L.; Ren, J.; Yang, H. Preparation and CO_2 capture properties of nanocrystalline Li_2ZrO_3 via an epoxide-mediated sol–gel process. *J. Sol-Gel Sci. Technol.* **2016**, *3*, 844–849. [CrossRef]

36. Zagorowsky, G.; Prikhod'ko, G.; Ogenko, V.; Koval'chuk, G. Investigation of kinetics of solid-phase synthesis of lithium orthosilicate. *J. Therm. Anal. Calorim.* **1999**, *55*, 699–705. [CrossRef]

37. Mohammed, H.I.; Garba, K.; Ahmed, S.I.; Abubakar, L.G. Thermodynamics and kinetics of Doum (Hyphaene thebaica) shell using thermogravimetric analysis: A study on pyrolysis pathway to produce bioenergy. *Renew. Energy* **2022**, *200*, 1275–1285. [CrossRef]

38. Kuznetsova, S.A.e.; Khalipova, O.g.S.; Lisitsa, K.V.; Ditts, A.A.; Malchik, A.G.e.; Kozik, V.V.e. Synthesis of nanostructured composite materials of MoO_3/TiO_2-SiO_2 with spherical shape prepared with resins. *Nanosyst. Phys. Chem. Math.* **2021**, *12*, 232–245. [CrossRef]

39. Karelin, V.A.; Voroshilov, F.A.; Strashko, A.N.; Sazonov, A.V.; Karelina, N.V. Fluorination of rutile, electrochemical reduction of titanium fluoride to titanium, and its separation from the electrolyte salts melt. *J. Chem. Technol. Metall.* **2020**, *55*, 1111–1119.

40. Wang, K.; Guo, X.; Zhao, P.; Wang, F.; Zheng, C. High temperature capture of CO_2 on lithium-based sorbents from rice husk ash. *J. Hazard. Mater.* **2011**, *189*, 301–307. [CrossRef] [PubMed]

41. Ida, J.i.; Xiong, R.; Lin, Y.S. Synthesis and CO_2 sorption properties of pure and modified lithium zirconate. *Sep. Purif. Technol.* **2004**, *36*, 41–51. [CrossRef]